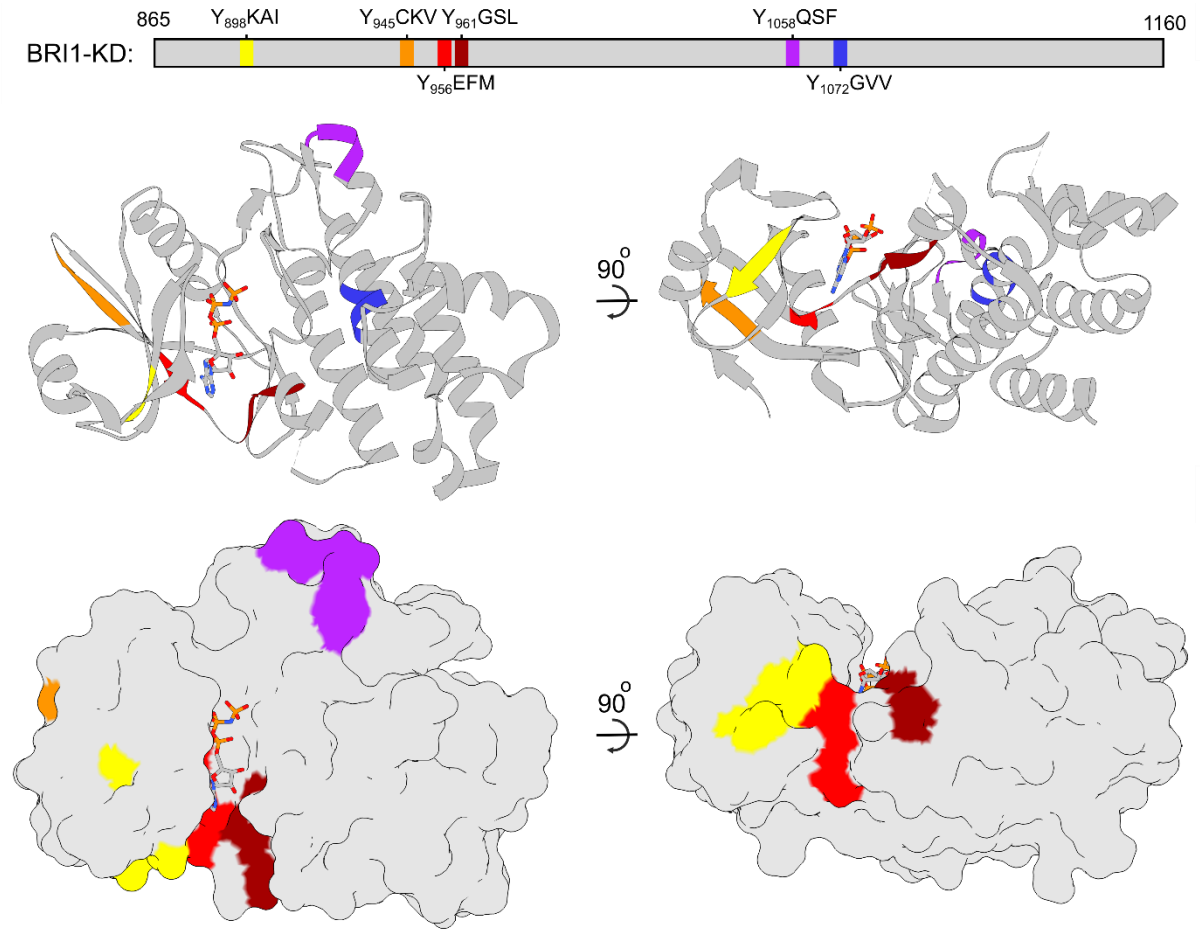


**Supplemental Figure 1.** Cartoon and Surface Representation of the Putative Endocytic YXXΦ Motifs in the BRI1 Kinase Domain (Supports Figure 2).
Canonical endocytic YXXΦ motifs are mapped on cartoon (middle) and surface (bottom) representations of the crystal structure of BRI1-kinase domain (KD) (PDB-ID, 5LPY). Colors corresponding to each YxxΦ motif are indicated on a linear scheme of BRI1-KD (top). Cyclic adenosine monophosphate (cAMP) is shown as sticks.


**Supplemental Figure 2.** Multiple Sequence Alignment of the µ-homology Domain (MHD) of AP2M (Supports Figure 2).
The amino acid sequences of AP2M-MHD from *Arabidopsis thaliana* (*At*AP2M-MHD) (amino acids 177 to 438) and *Homo sapiens* (*Hs*AP2M-MHD) (amino acids 170 to 436) were aligned by means of the Clustal Omega server (https://www.ebi.ac.uk/Tools/msa/clustalo/). The conserved $D_{176}$ and $W_{421}$ in the human AP2M-MHD corresponding to $D_{183}$ and $W_{424}$ in the *Arabidopsis* AP2M-MHD are highlighted in blue. Numbers represent the amino acid positions. Asterisks, colons and periods indicate identical, similar, and semi-similar amino acids, respectively. Dashes represent gaps introduced to allow optimal alignment.

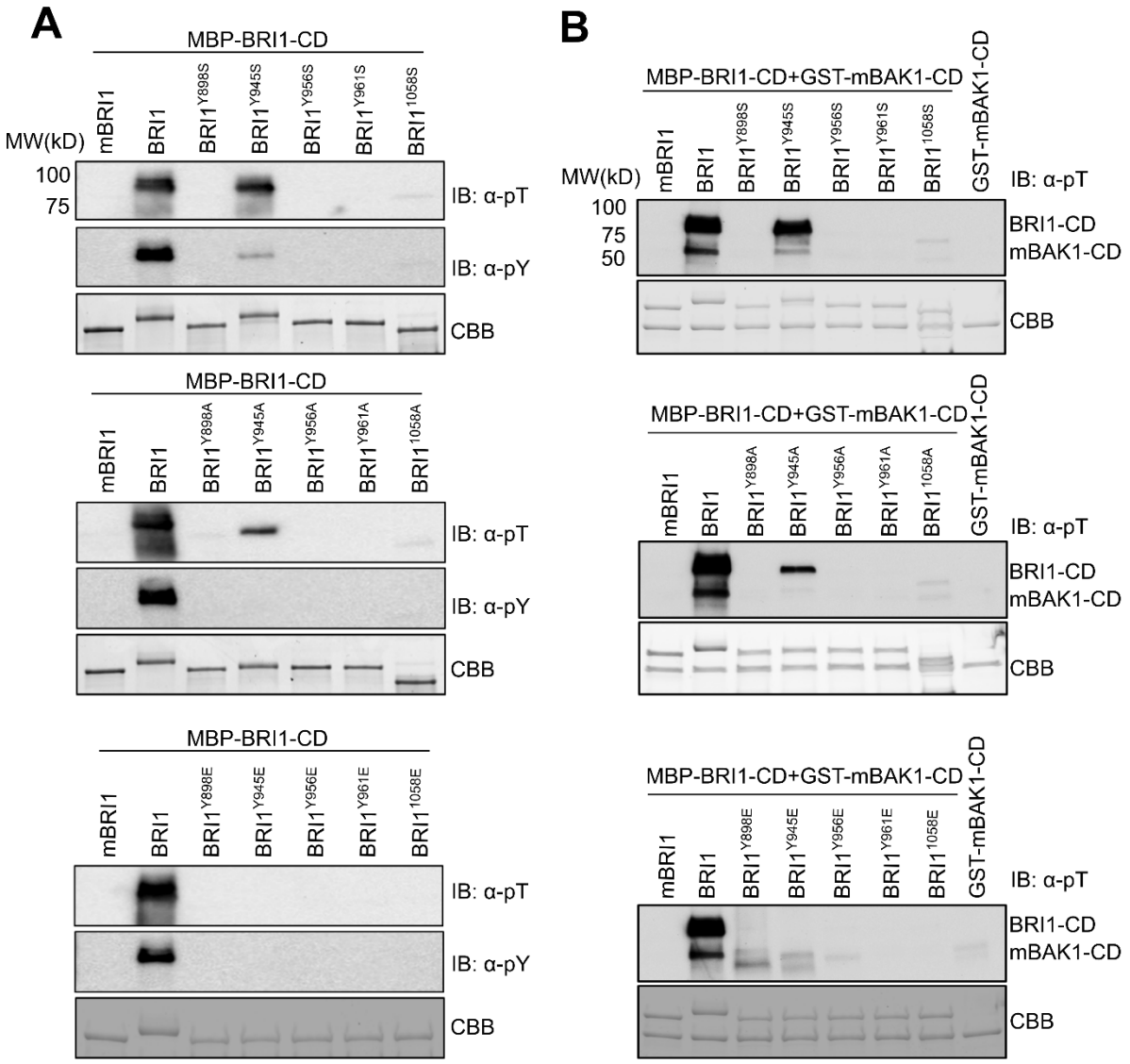


**Supplemental Figure 3.** The *in vitro* Kinase Activity of BRI1 Is Impaired by Substitution of the Tyrosine (Y) by Serine (S), Alanine (A) or Glutamic Acid (E) in the Putative YXXΦ Motifs (Supports Figure 2 and Figure 3).

Effect of site-directed mutagenesis of the Y residues into S, A and E in BRI1-cytoplasmic domain (CD) on autophosphorylation **(A)** and on transphosphorylation of BAK1 **(B)**. Equal amounts of recombinant MBP tagged wild type, Y-to-S, Y-to-A and Y-to-E mutated and inactive ($BRI1^{K911E}$, mBRI1) BRI1 CDs were loaded and detected by immunoblotting (IB) with the α-pT and α-pY antibodies **(A)** or they were combined with GST-tagged inactive BAK1 (mBAK1) CD in a kinase assay followed by IB detection with the α-pT antibody **(B)**. Coomassie Brilliant Blue (CBB) staining was used as a loading control.

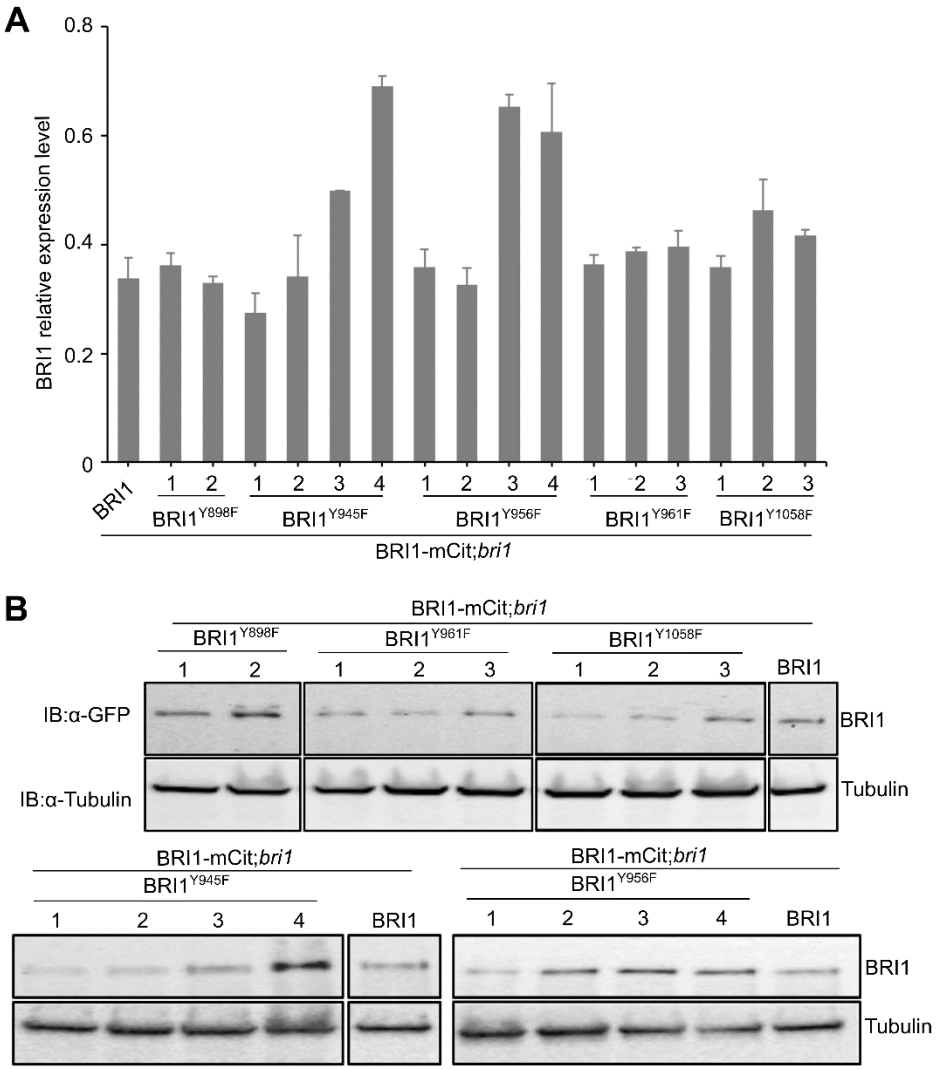


**Supplemental Figure 4.** Molecular Characterization of the *Arabidopsis* Transgenic Lines Harboring Y-to-F Mutations in the Putative YXXΦ Motifs in BRI1 (Supports Figure 3).

**(A)** Real-time quantitative reverse transcription PCR (qRT-PCR) analysis of *BRI1* (*n* = 3, biological replicates). Total RNA was isolated from 5-day-old seedlings of two to four independent transgenic lines. The expression of *ACTIN4* was used as an internal control. Error bars indicate s.d. (*n* = 3, biological replicates [independent experiments]).

**(B)** Immunoblotting (IB) analysis of the *BRI1* expression. Total proteins were isolated from 5-day-old seedlings of the transgenic lines and BRI1-mCitrine (mCit); *bri1* and detected with the α-GFP antibody (top). The protein inputs were equilibrated by IB with the α-tubulin antibody (bottom).

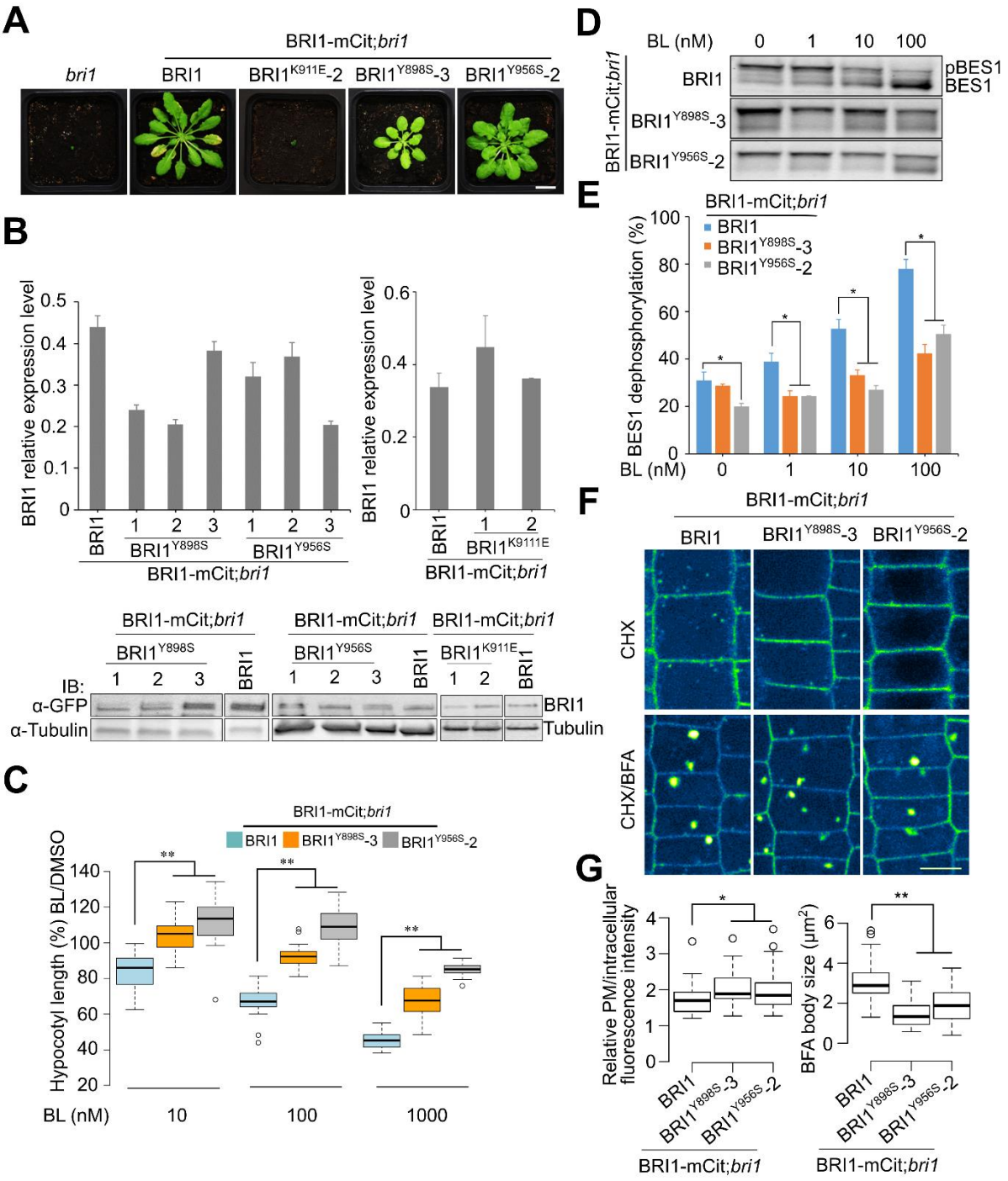


**Supplemental Figure 5.** Transgenic Lines Harboring Y-to-S Mutations at $Y_{898}$ or $Y_{956}$ in BRI1 Are Resistant to BRs and Exhibit Impaired BRI1 Internalization (Supports Figure 3 and Figure 4).

**(A)** Growth phenotype of 6-week-old soil-grown plants.

**(B)** Molecular characterization of the *Arabidopsis* transgenic lines harboring the indicated mutations in BRI1. Total RNA or protein was isolated from 5-day-old seedlings, followed by real-time quantitative reverse transcription PCR (qRT-PCR) or immunoblotting (IB) with α-GFP and α-tubulin antibodies to detect BRI1 expression or protein loading, respectively. Error bars indicate s.d. (*n* = 3, biological replicates [independent experiments]).

**(C)** Average hypocotyl length (normalized to DMSO) of 5-day-old seedlings grown in the dark and in the presence of increasing concentrations of brassinolide (BL). At least 15 seedlings were measured for each line and each treatment.
**(D)** BES1 dephosphorylation assay of 5-day-old seedlings treated with different concentrations of BL for 1 h.
**(E)** Percentage of dephosphorylated BES1 relative to total BES1 from three independent experiments. Error bars indicate s.d. ($n$ = 2, biological replicates [independent experiments]). $P$ values (Student's $t$-test), * <0.05 relative to BRI1-mCit;*bri1*.
**(F)** and **(G)** Y898S and Y956S mutations impaired BRI1 endocytosis. Epidermal cells from the root meristems of 5-day-old seedlings treated with cycloheximide (CHX) (50 µM) for 1.5 h (top panel) or pre-treated with CHX for 1 h, followed by a treatment for 30 min with CHX and Brefeldin A (BFA) (50 µM) (bottom panel) **(F)** relative plasma membrane (PM) BRI1-mCitine (mCit) fluorescence and BFA body size **(G)**. For each line, at least 25 cells from five seedlings were measured.
Box plots in **(C)** and **(G)** show the first and third quartiles, split by the medians (lines), with whiskers extending 1.5-fold interquartile range beyond the box. $P$ values (one-way ANOVA and Tukey's post hoc) * <0.05; ** <0.01 relative to BRI1-mCit;*bri1* in **(C)** and **(G)**. Scale bars, 2 cm **(A)**, 5 µm **(F)**.

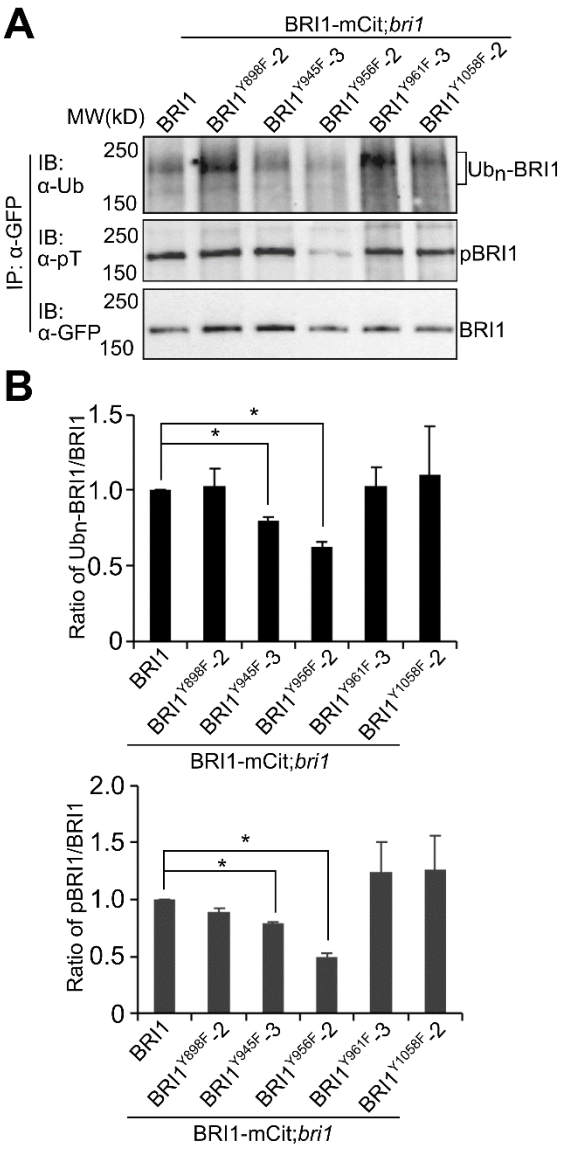


**Supplemental Figure 6.** Phosphorylation and Ubiquitination Profile of BRI1 Y-to-F Mutants *in vivo* (Supports Figure 3).

**(A)** Isolation of microsomal fractions from 6-day-old seedlings treated with 2 µM brassinazole (BRZ) for 24 h followed by a treatment with 100 nM brassinolide (BL) for 1 h. BRI1 was immunoprecipitated with GFP-Trap-Magnetic Agarose and subjected to immunoblotting (IB) with α-Ub (P4D1) (top), α-pT (middle) or α-GFP (bottom) antibodies.

**(B)** BRI1 ubiquitination ($Ub_n$-BRI1/BRI1) and phosphorylation (pBRI1/BRI1) profiles. Error bars indicate s.d. (*n* = 2, biological replicates [independent experiments]). *P* values (Student's *t*-test) * <0.05 relative to BRI1- mCit;*bri1*.

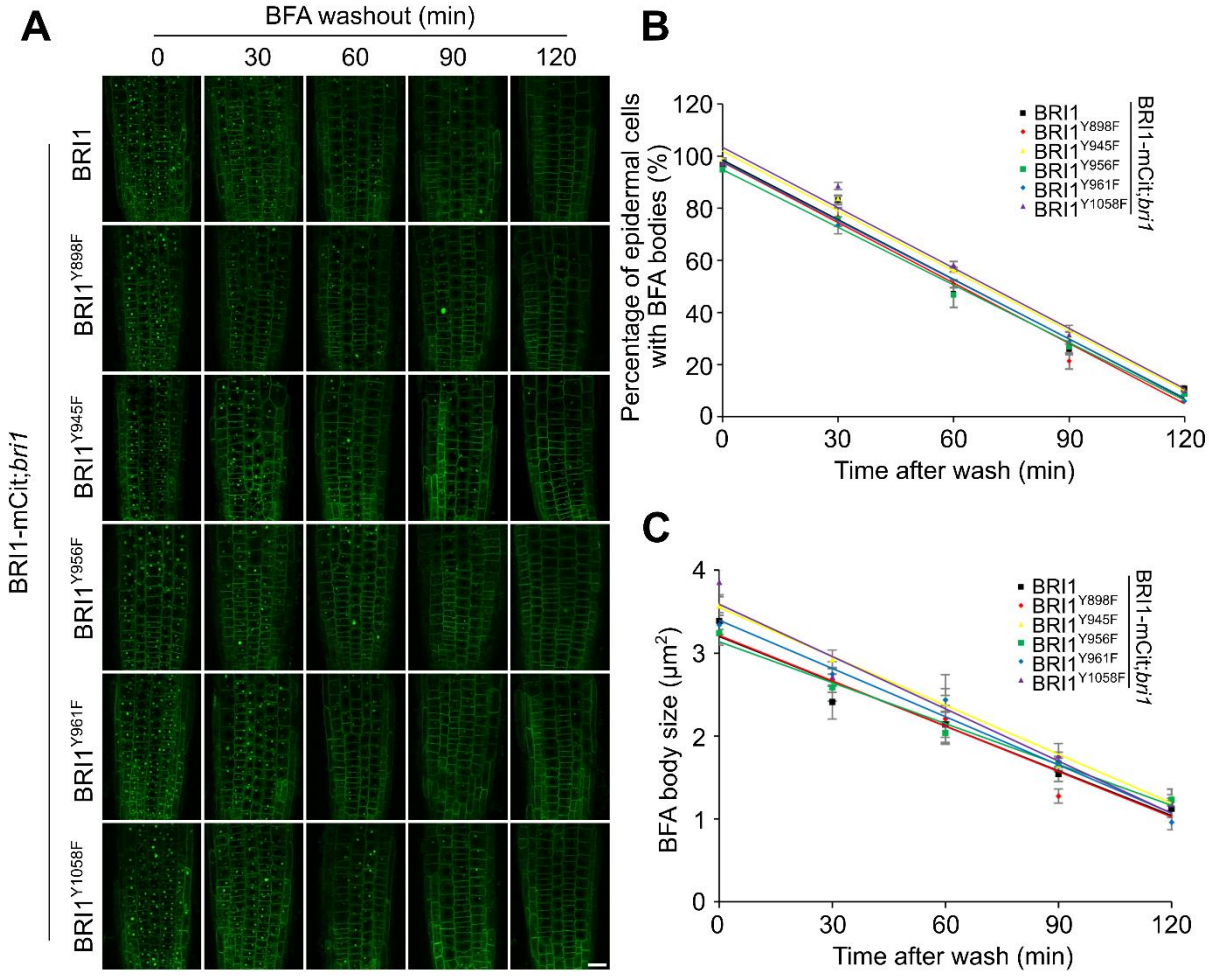


**Supplemental Figure 7.** Y-to-F Mutations in the Putative YXXΦ Motifs in BRI1 Do Not Affect BRI1 Recycling (Supports Figure 4).

**(A)** Images of root meristem epidermal cells of 5-day-old *Arabidopsis* seedlings pre-treated with cycloheximide (CHX) for 1 h, followed by a combined treatment with CHX plus Brefeldin A (BFA) for 30 min. Seedlings were imaged at 0, 30, 60, 90, and 120 min after BFA washout in CHX. Scale bar, 20 μm.

**(B)** and **(C)** BRI1-mCitrine (mCit) re-localization from the BFA bodies to PM was quantified by percentage of epidermal cells with BFA bodies **(B)** or by BFA body size **(C)**. **(B)** and **(C)** Error bars indicate s.d. **(B)** ($n$ = 3, roots); **(C)** ($n$ > 20, BFA bodies). For each treatment at least three seedlings were imaged and quantified. Experiments were performed twice, and similar results were obtained.

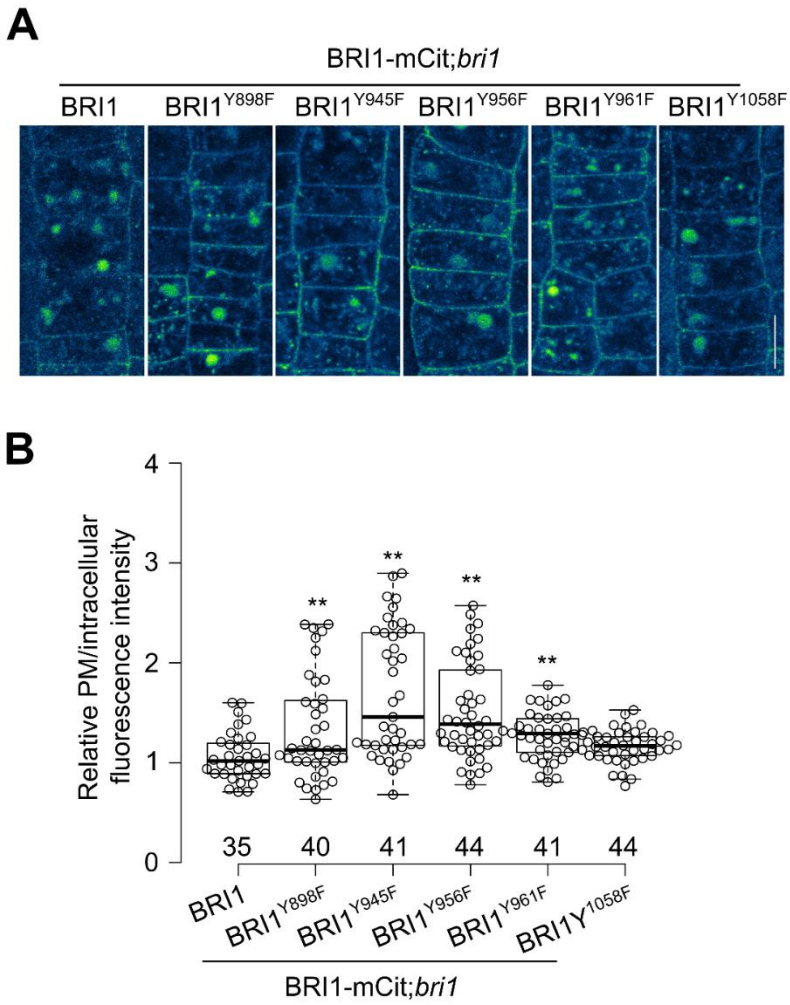


**Supplemental Figure 8.** The Vacuolar Targeting of BRI1 in the Transgenic Lines Harboring Y-to-F Mutations in $Y_{898}$, $Y_{945}$, $Y_{956}$ and $Y_{961}$ Residues is Impaired (Supports Figure 4).

**(A)** Images of root meristem epidermal cells from constant light-grown 5-day-old seedlings that were kept in darkness for 4 h before confocal imaging. Green fire blue LUT was applied to the images to enhance contrast and highlight the differences between different transgenic lines. Scale bar, 10 μm.

**(B)** Measurements of the relative plasma membrane (PM)/intracellular BRI1-mCitrine (mCit) fluorescence intensity. For each transgenic line, at least 35 cells from five seedlings were measured. Box plots show the first and third quartiles, split by the medians (lines), with whiskers extending 1.5-fold interquartile range beyond the box. *P* values (one-way ANOVA and Tukey's post hoc) ** <0.01 relative to BRI1-mCit;*bri1*. Experiments were performed twice and similar results were obtained.

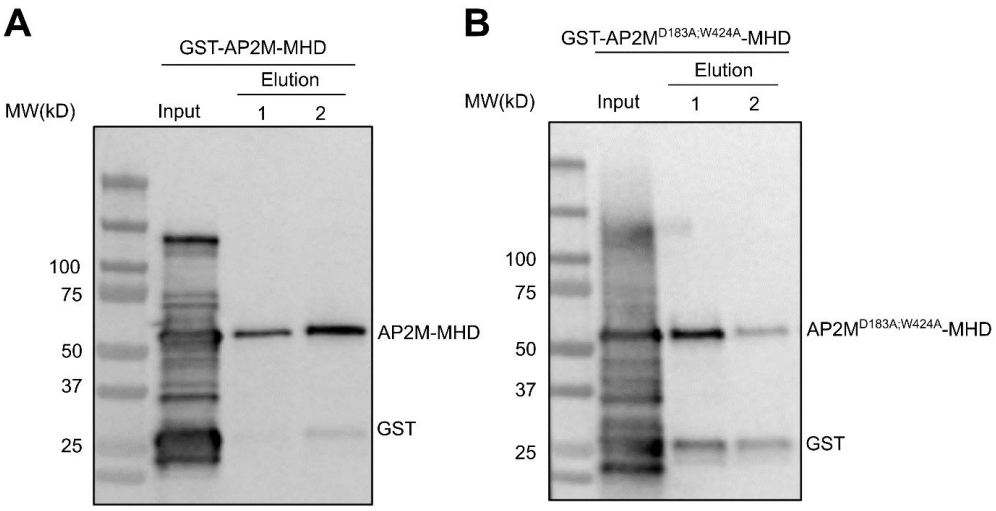


**Supplemental Figure 9.** Purification of GST-tagged AP2M-μ Homology Domain (MHD) (Supports Figure 5).
Two elution fractions, collected for GST-AP2M-MHD **(A)** and GST-AP2M-MHD$^{D183A;W424A}$ **(B)** purified by size-exclusion chromatography and glutathione resin, were stained together with the input (the total protein isolated from the *E. coli* pellet before purification) with Coomassie Brilliant Blue (CBB).

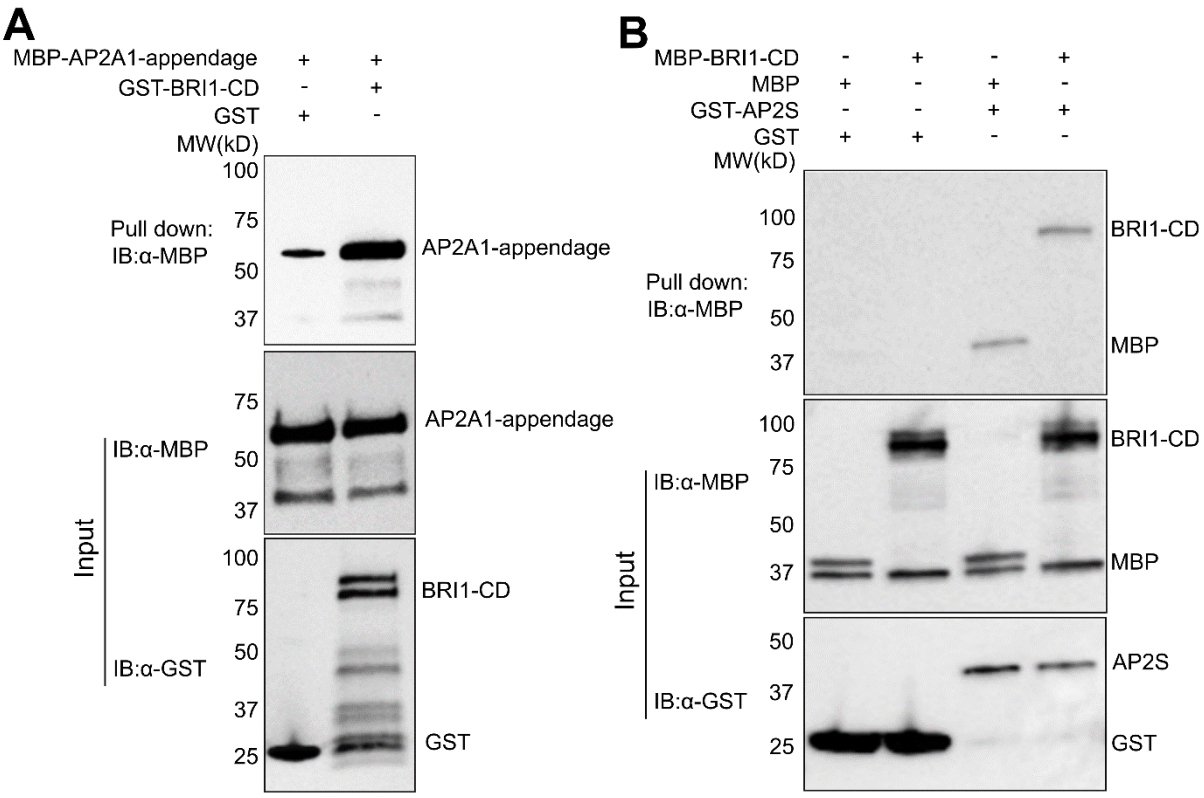


**Supplemental Figure 10.** BRI1 Interacts Directly with AP2A1 and AP2S *in vitro* in GST Pull-down Assays (Supports Figure 1).

(**A**) BRI1 interacts with the AP2A1 appendage domain. The MBP-fused AP2A1 appendage domain (MBP-AP2A1 appendage) was incubated with glutathione beads coupled with GST or GST-BRI1-CD, whereafter the beads were collected and washed, followed by immunoblotting (IB) with α-MBP antibodies.

(**B**) BRI1 interacts with AP2S. MBP or MBP-BRI1-CD were incubated with glutathione beads coupled with GST or GST-AP2S, whereafter the beads were collected and washed. The protein inputs were determined by IB with α-GST and α-MBP antibodies.

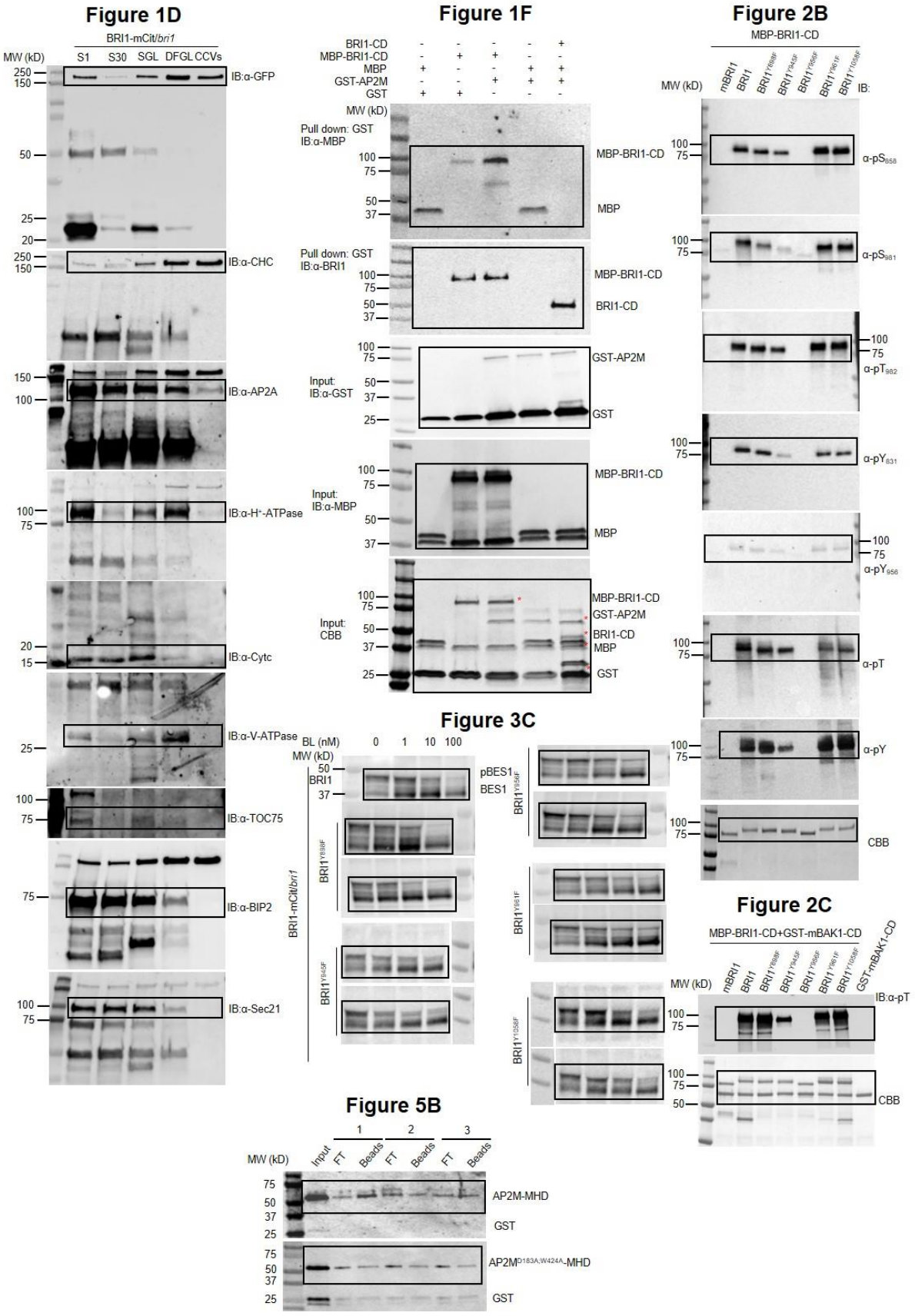


**Supplemental Figure 11.** Original Blots (part 1) (Supports Figure 1, Figure 2, Figure 3, and Figure 5).

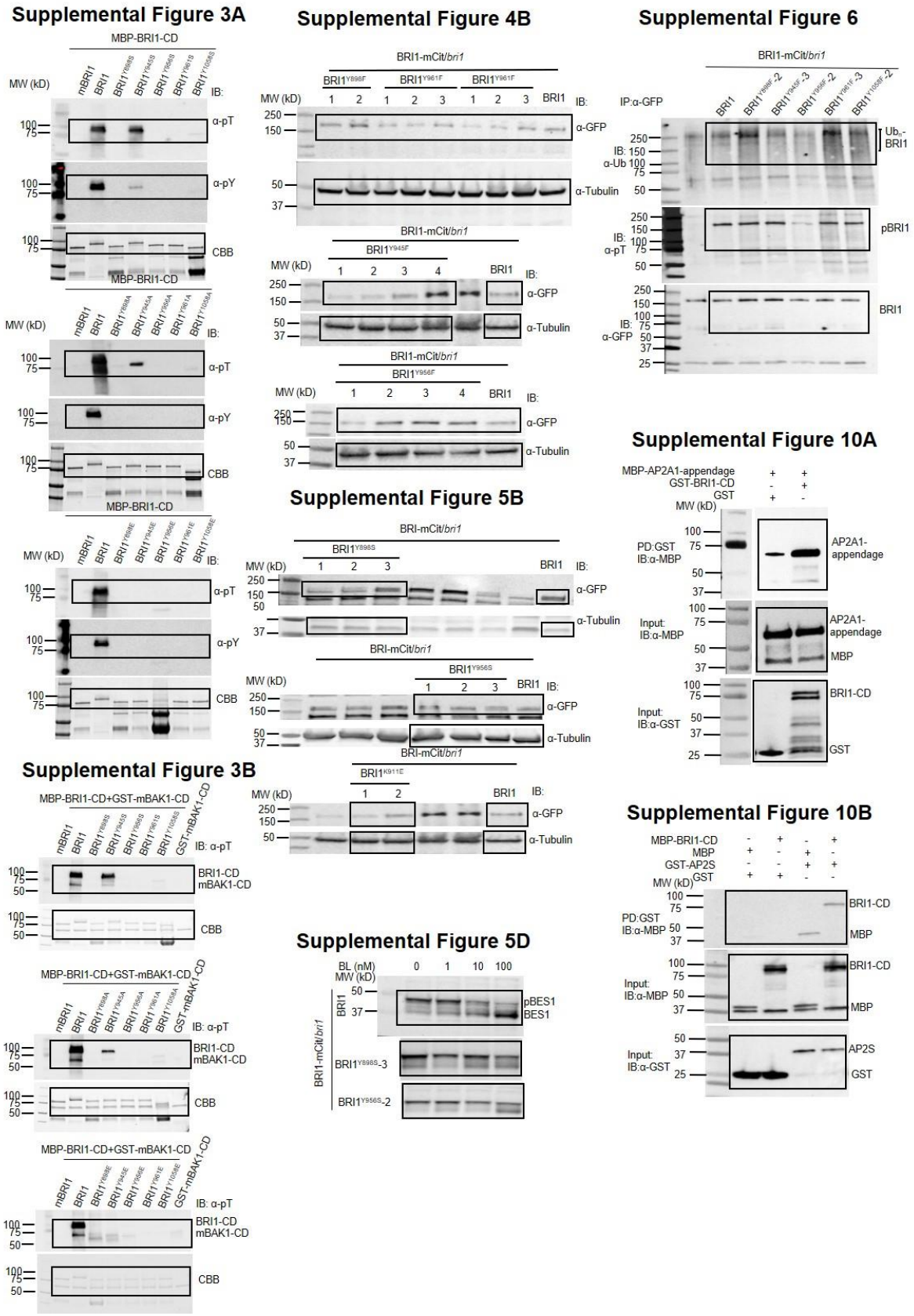


**Supplemental Figure 11.** Original Blots (part 2). (Supports Supplemental Figure 3, Supplemental Figure 4, Supplemental Figure 5, Supplemental Figure 6 and Supplemental Figure 10).